Taylor & Francis
Taylor & Francis Group

Buckling of a tilted line of confined hard spheres

Q1   A. Irannezhad [a], D. Weaire[a], A. Mughal[b], J. Ryan-Purcell[a] and S. Hutzler[a]

[a]School of Physics, Trinity College Dublin, The University of Dublin, Dublin, Ireland; [b]Department of Mathematics, Aberystwyth University, Penglais, UK

ABSTRACT

A linear chain of hard spheres confined in a transverse harmonic potential is unstable and buckles, if tilted beyond some critical angle. We examine this symmetry breaking using a computational model that was previously applied to buckling under compression. Results are presented in a bifurcation diagram (in terms of energy as a function of tilt), including both stable and unstable equilibrium states. The key results are consistent with experiments using metal spheres resting in a cylinder.

1. Introduction

A finite compression of a straight linear chain of hard spheres results in buckling, that is, lateral displacements of the spheres. The profile of these displacements is arbitrary but it is reproducible if a confining potential is imposed on all spheres, opposing their lateral displacement. (In what follows the potential will be harmonic.) With this addition, the system exhibits a bucking profile that varies with compression and takes multiple forms at high compression.

This constitutes an interesting nonlinear system, amenable to computation and experiment, at various levels of sophistication. We have investigated it systematically in a series of papers that deal with mainly buckling profiles, which exhibit interesting localisation properties [1–5]. A wealth of computed results was gathered together in bifurcation diagrams, indicating the energies or position of (stable and unstable) equilibrium states, for a range of compressions. Initially these results were interpreted in terms of direct simulations of discrete systems of up to 20 spheres, whose centres are confined to two dimensions, but an approximate *continuous description*, making connections with Jacobi functions, was eventually found to be helpful [5].

At low compression the system buckles in the form of a *zig-zag* arrangement, with a smooth profile (depending on boundary conditions). This is modulated to form a more localised concentration of displacement at higher compression (see Figure 1).

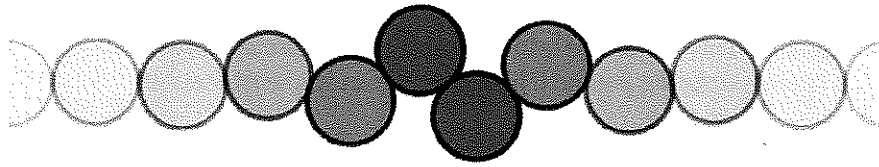**CONTACT** A. Irannezhad ✉ iranneza@tcd.ie

Figure 1. Localised buckling in a linear chain of spheres.

In further work, a longitudinal force was introduced, acting on each sphere, as may be produced, in practice, by *tilting* the apparatus (so that a component of gravity plays the role of the longitudinal force). The movement of localised buckling concentration (called 'kinks' or 'solitons' in some related fields) under the influence of the longitudinal force, is of further interest, in relation to Peierls–Nabarro potentials [4]. These are of relevance to arrangements of trapped ions [6], which are of particular current interest in relation to quantum computing [7].

In the present paper, we retreat towards the low compression regime, typically dealing with a configuration as in Figure 2. Whereas in absence of a longitudinal (tilt) force, buckling arises at infinitesimal compression, here it occurs at
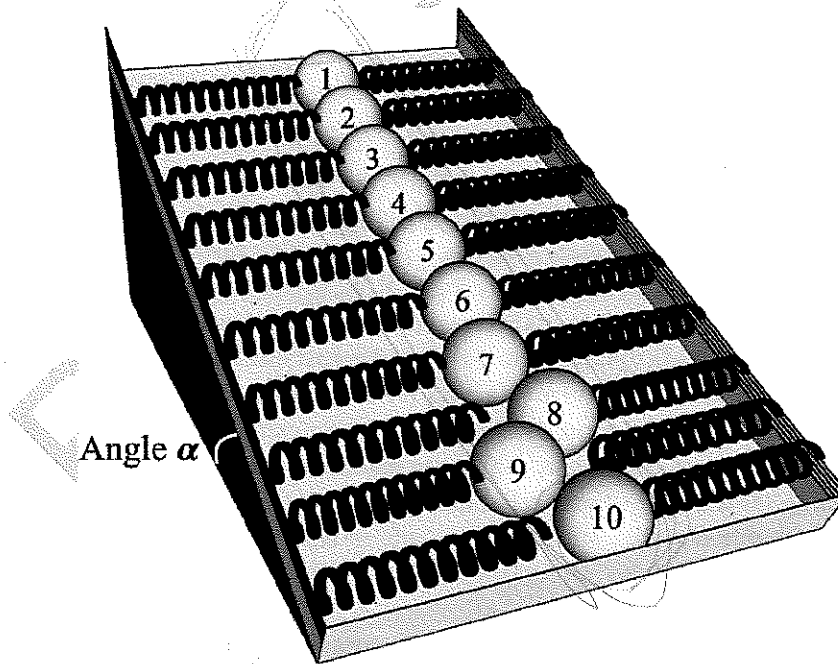

Figure 2. Schematic illustration of the model used in this paper, i.e. a tilted line of spheres in a harmonic confining potential, with the final sphere (here $N = 10$) in contact with a hard wall. A tilt by an angle a beyond a critical value leads to a buckling of the initially linear chain; transverse sphere displacement results in a harmonic restoring force.

a finite critical value of tilt, if there is no confining boundary at the upper end of the system (see Figure 2). This is analogous to the buckling/collapse of a tower under gravity, the lateral confining potential being analogous to the *stiffness* of the tower.

Determining the critical tilt for a chosen case (number N of spheres) is straightforward, but we will broaden the question to include the nature of the buckling transition and other related buckling states, which are gathered together in Figure 4.

We will have cause to mention the continuous formulation which we have previously developed [3, 5], corroborating many of the findings included here. The continuous description raises several detailed theoretical questions: accordingly we are deferring it to another publication [8] and will touch on its results only briefly in what follows.

The scenario which emerges should be compared with experiment, but this has proved difficult. We present only some limited results in Section 5. The difficulty arises from the inevitable frictional forces between ordinary hard spheres (ball bearings). It may be obviated by instead using bubbles [2], but these are deformable, so that theory would need to be extended to that case; which we anticipate in this future work.

2. Theoretical and computational methods

2.1. Modelling the discrete system

A chain of N contacting identical hard spheres is tilted to make contact with a hard wall, as illustrated in Figure 2, and shown in the plane of tilt in Figure 3. Displacement of a sphere by a distance R_n away from the central axis results in a transverse restoring force F_n with magnitude kR_n, where k is a spring constant. We introduce non-dimensional quantities by defining $r_n = R_n/D$, where D is the sphere diameter. The dimensionless transverse force f_n is defined as $f_n = F_n/(kD)$. Inserting for F_n leads to $f_n = r_n$; in our non-dimensional formulation the magnitude of the transverse force f_n acting on a sphere equals its transverse displacement r_n, a positive quantity. See Figure 3 for notation.

In a chain which is tilted by an angle α, each sphere of mass m experiences a tilt force $mg \sin \alpha$ along the axial direction. In the following, we introduce the non-dimensional tilt variable τ by

$$\tau = mg \sin \alpha / (kD). \tag{1}$$

The centres of contacting spheres are separated by their diameter. Hence in our dimensionless variables the radial distances and forces are given by

$$f_n + f_{n+1} = r_n + r_{n+1} = \sin \theta_n, \tag{2}$$

see Figure 3.

Top view

Figure 3. Top view of the buckled chain of Figure 2, with relevant notation of the dimensionless quantities, as defined in the main text. The forces f_n (equivalent to the dimensionless displacements) are due to the confining potential, g_n are the compressive forces at sphere-sphere contacts). The sphere positions in this example were obtained from computer simulations for the dimensionless tilt, $\tau = 0.03$.

The angles between successive sphere centres play an important role. They alternate in sign in a zig-zag structure, but a factor $(-1)^n$ is included in the variable θ_n used here; this remains positive in the main cases discussed below; similarly the alternation of sign is suppressed in the transverse displacement f_n [3,5]. The applied (hard wall) boundary conditions correspond to $\theta_0 = \theta_N = 0$.

In the presence of tilt, the (non-dimensional) compressive force g_n between contacting spheres depends on the position of a sphere within the chain,

$$g_n \cos \theta_{n-1} = \tau(n-1), \tag{3}$$

where τ is our tilt variable. (In our previous work for $\tau = 0$ the right-hand side of Equation (3) was replaced by a constant compressive force [3,5]).

From the transverse force balance for the displaced nth sphere we obtain

$$\tan \theta_n = \frac{f_n - (\tau(n-1))\tan \theta_{n-1}}{\tau n}. \tag{4}$$

The boundary condition for sphere $n = 1$ requires θ_0 to be zero, with an arbitrary f_1. Using Equations (2) and (4) we proceed iteratively to (f_{n+1}, θ_{n+1}). The angle θ_N corresponds to the contact of the Nth sphere with the wall, which can be made equal to zero by adjusting the value of f_1 using a shooting method, as in [1,3].

The total energy is the sum of the energy due to transverse sphere displacement, $\frac{1}{2} k D^2 \sum_{n=1}^{N} R_n^2$, and the energy due to tilt, $mg \sin \alpha \sum_{n=1}^{N} x_n$. Here x_n is the position along the central axis of sphere n, given by $x_n = D(\frac{1}{2} + \sum_{i=1}^{N-n} \cos \theta_{N-i})$. Evaluation of the double sum and division of both energy contributions by kD^2 results in the following expression for the

non-dimensional energy E for a chain of N spheres,

$$E = \frac{1}{2}\sum_{n=1}^{N} r_n^2 + \tau\left(\sum_{n=0}^{N}(n\cos\theta_n) - \frac{N}{2}\right). \qquad (5)$$

2.2. Energy minimisation

In the following, we also have recourse to modelling the chain of spheres as deformable with purely repulsive harmonic forces, as commonly used in computational studies of jamming [9]. This allows for overlaps between spheres, leading to a penalty in the total energy. The total energy (which varies quadratically with overlap) can readily be minimised with respect to the coordinates of the sphere centres (using for example conjugate gradient based methods) to find the equilibrium state of lowest energy.

To make contact with our hard sphere simulations (which are based on the iterative method, Section 2.1) we set the magnitude of the elastic force between spheres to be 50 times greater than the transverse force. This leads to a deviation from the ideal hard sphere model which is negligible for our purpose here. The deviation from the ideal hard-sphere model may be gauged by considering the doublet structure (an example of which is shown in Figure 4 by the chain of red spheres), where the displacement of two contacting transverse hard spheres is
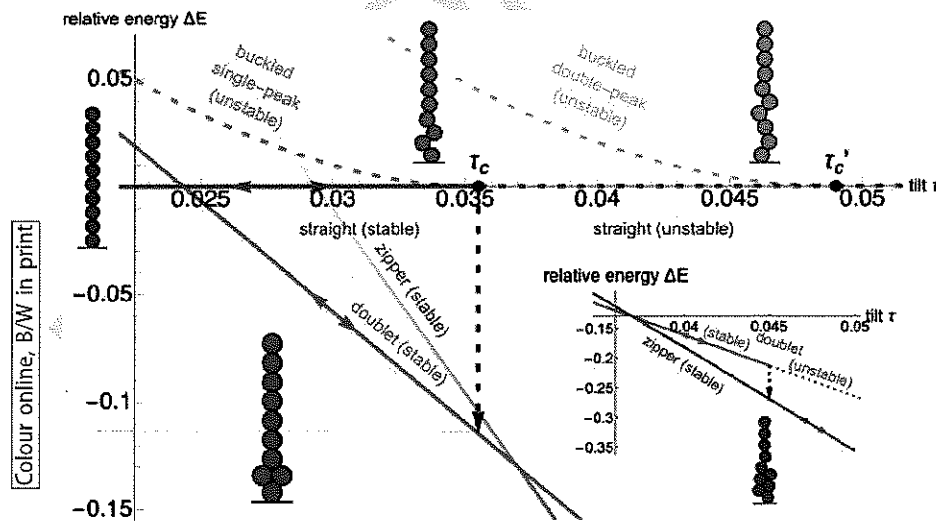
Figure 4. Bifurcation diagram for a system with $N = 10$, obtained from simulations, see Section 2. Shown is the variation of the energy difference $\Delta E = E - E_s$ of total energy E (Equation 5) and energy of the straight chain, E_s, as a function of tilt τ. Examples of the various structures described in the text are shown, with arrows indicating allowed directions of change of stable solutions. The transition from the doublet to the zipper structure is shown in close-up in an inset.

exactly a half and next-nearest neighbour contacts have formed; with our choice of the elastic force between contacting spheres this displacement differs from this value by less than $\frac{1}{4}$ percent.

3. Results of simulations

We first address the question: *what happens if the tilt is gradually increased from zero?*

It may be obvious that a *small* tilt will not render the chain unstable. We expect it to become unstable with respect to buckling at some critical value of tilt, $\tau = \tau_c$. We wish to determine τ_c (for specified N, the number of spheres) and describe what happens around the critical point. As an example, we choose $N = 10$, for which results are shown in Figure 4.

It is trivial to derive the energy of a straight chain (whether stable or not), $E_s = \tau N^2/2$, and we subtract this from calculated energies E (Equation (5)), for simplicity of presentation,

$$\Delta E = E - E_s. \tag{6}$$

Hence the horizontal axis in Figure 4 represents the straight chain solution, which is stable in the range $0 < \tau < \tau_c$, where $\tau_c = 0.03557$ (as determined by using the stepwise method of Section 2), and unstable for higher values of τ.

One might have expected a bifurcation at the critical point τ_c such that a branch emerges that corresponds to a buckled solution, developing as τ is further increased, as in the classic description of Euler buckling of a beam. This is not the case here; there is no such 'forward branch', but rather a 'backward' one, which one may readily identify as *unstable*. In later sections, we will explore its nature. For now, let us ask: what happens to the stable system when τ reaches τ_c?

To answer this question we have had recourse to the deformable sphere model of Section 2.2. We equilibrate a linear chain of such spheres using gradient descent methods for energy minimisation and find that it is stable for $\tau < \tau_c$. Beyond this point, it falls into a doublet, if energy is minimised (see dashed black arrow in Figure 4). This type of state was encountered in our earlier study of buckling under compression [3]. The energy difference between the doublet structure and the linear chain is given analytically by

$$\Delta E_{doublet} = 1/4 - (3 - \sqrt{3})(N - 2)\tau. \tag{7}$$

If τ is now reduced, the system remains in the doublet state for $\tau < \tau_c$ and transitions to the linear chain only at $\tau = 0$. The stable straight chain with which we began this description is the state of lowest energy *only* for $\tau < 0.0246$ (from Equation 7). On the other hand, if τ is increased, the doublet structure develops into an extended double chain (which we will call a 'zipper'), similar to what
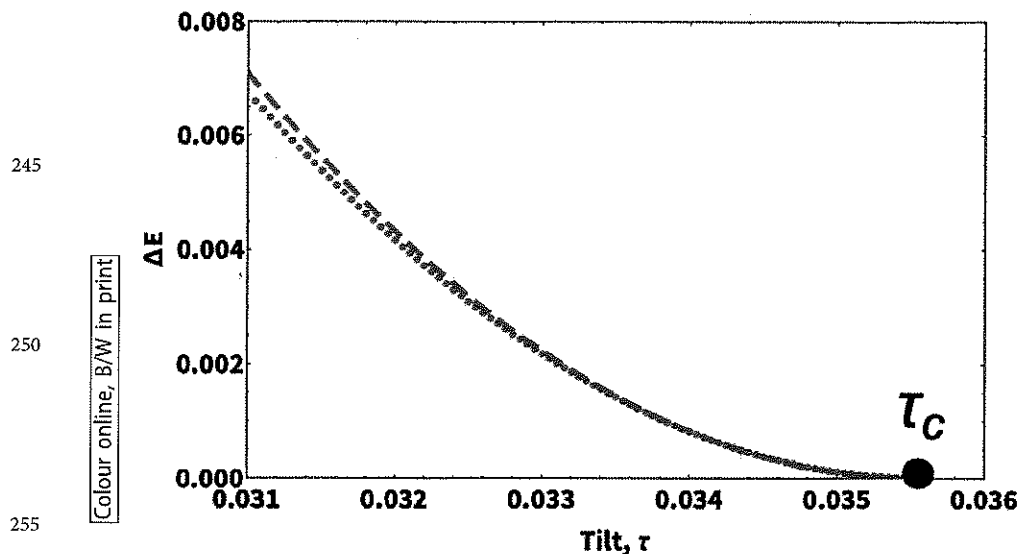
Figure 5. Close to the critical value of tilt, τ_c, the variation of the computed energy ΔE (Equation 6) (blue data points) for the unstable buckled structure indicated in Figure 4 is well fitted by a quadratic form (dashed red line). (Data shown is for $N = 10$.)

was found by Pickett *et al.* in computer simulations of cylindrically confined spheres [10].

For $\tau < \tau_c$ the bifurcation diagram includes the 'backward branch' corresponding to an unstable state. The variation of energy close to τ_c is quadratic for this state, as Figure 5 shows. The critical value of tilt (for $N = 10$) is $\tau_c = 0.03557$.

Figure 6(a) shows examples of profiles of displacements f_n for the unstable state, obtained from simulations of the discrete $N = 10$ chain, for values of tilt just below τ_c. The profiles are characterised by a long tail of near zero displacements, with a peak below the 9th sphere and a substantial displacement also for the 10th sphere, which is in contact with the wall. We will return to the interpretation of these profiles and their scaling in Section 4.3.

Our bifurcation diagram, Figure 4, shows also the variation of energy of an unstable higher energy double-peak structure, but we have not yet further analysed this state.

4. Further interpretation

4.1. Hessian eigenvalues and eigenvectors

To shed further light on the unstable states, we will in the following consider the Hessian matrix associated with the energy of a perturbed straight chain for values of τ around τ_c. As usual, positive eigenvalues are associated with stable modes of deformation, while negative ones denote instability.
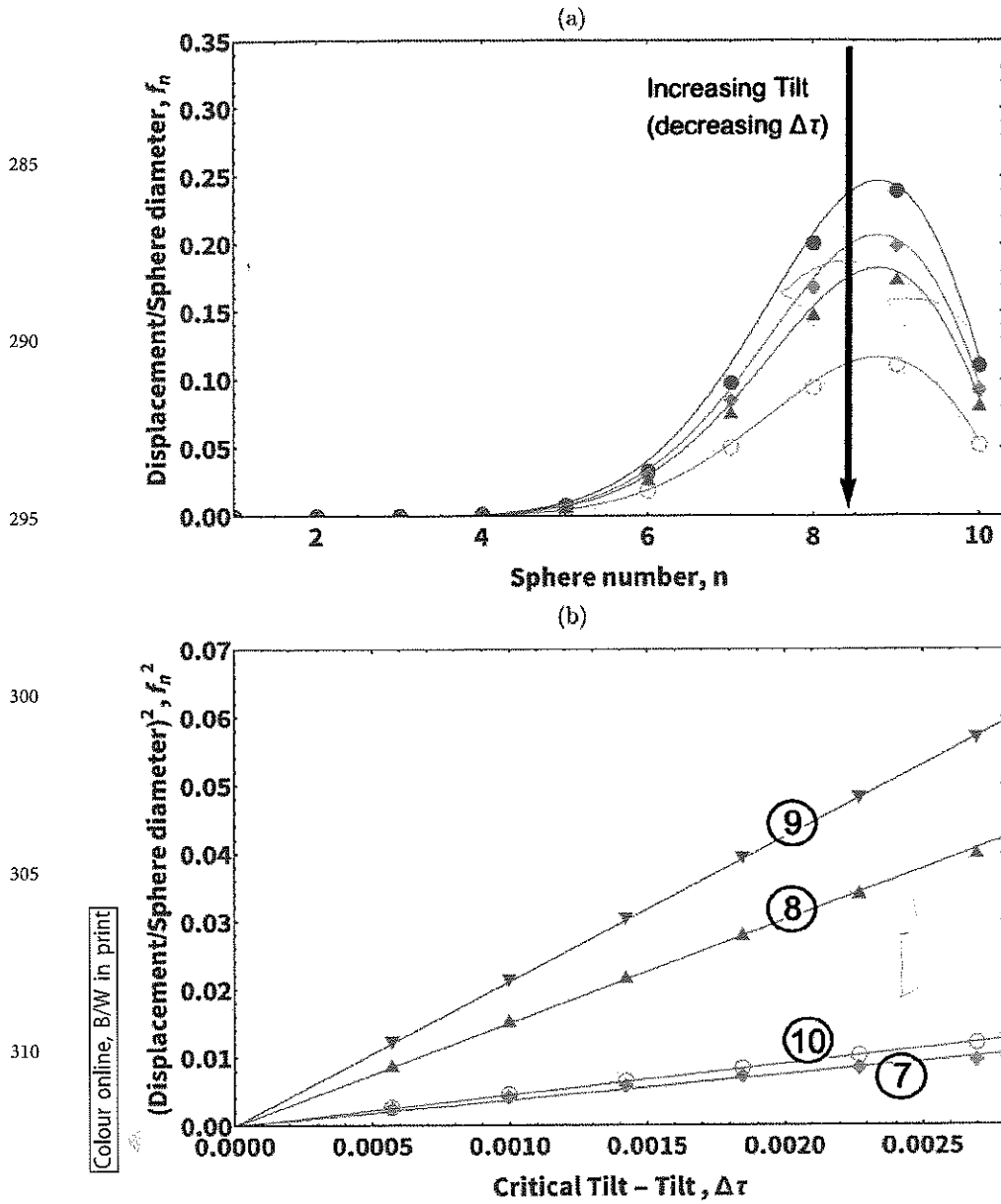
(a)

(b)

Figure 6. Simulation results for the (unstable) single peak solution shown in Figure 4. (a) Displacement profiles for values $\Delta\tau = \tau_c - \tau$ close to τ_c ($\Delta\tau = 0.0055, 0.0030, 0.0017, 0.0005$). The data points result from the discrete calculations (using the stepwise method), the solid lines are analytic solutions obtained from the continuum model, involving the Whittaker function; see Section 4.3. (b) Square of the displacement, taken at spheres 7, 8, 9, 10, respectively, as a function of $\Delta\tau$. The linear scaling of the *square* of the displacement with $\Delta\tau$ is also reproduced in the simple heuristic model of Section 4.2 and the continuum model (Section 4.3).

The hard sphere model makes use of generalised coordinates (in terms of θ_n and f_n) which guarantees that adjacent spheres cannot overlap. In the soft sphere model (Section 2.2), we do not have to explicitly impose hard-sphere constraints to prevent overlaps between spheres. Instead, these constraints are approximated (to a good degree) by the imposition of an overlap penalty in the energy. Therefore, we are free to specify the sphere centres using Cartesian coordinates. The resulting expression for the energy of the system and the Hessian (i.e. the matrix of second derivatives of the energy with respect to the coordinates) has an exceptionally simple form in terms of Cartesian coordinates, making the computation of eigenvalues and eigenvectors straightforward.

Figure 7 shows the lowest three eigenvalues, λ_0, λ_1, λ_2, as a function of τ. The eigenvector for λ_0 corresponds to the displacement profile of the unstable solution, as shown in Figure 8.

4.2. Simple models

We can shed further light on the results with simple heuristic models as follows. The instability occurs where the local compressive force is largest, i.e. towards the bottom of the chain. Suppose we allow displacement of only the penultimate sphere, so that there is only a single variable (f, the displacement of the sphere, or θ, the angle associated with the line connecting the centres of the penultimate and the final sphere, which is in contact with the wall) describing the buckled
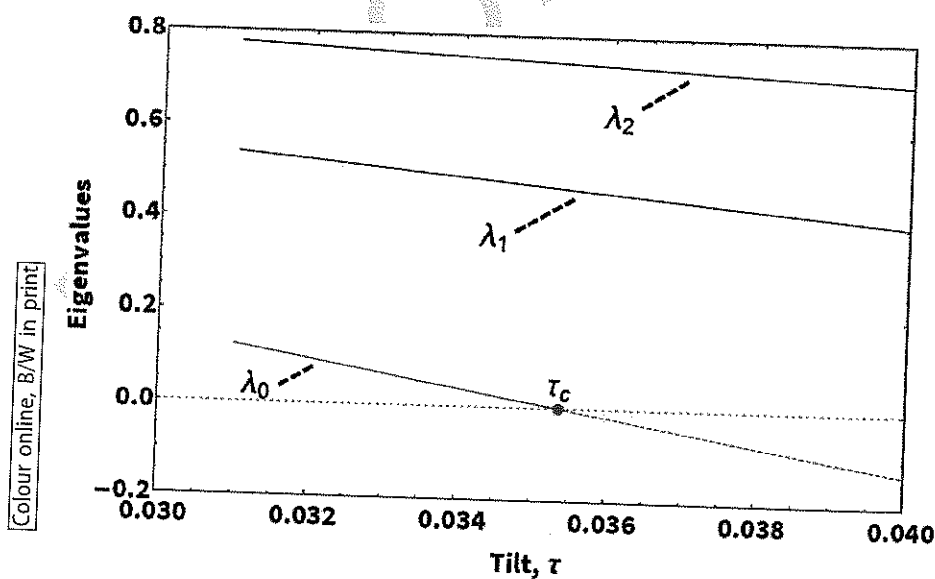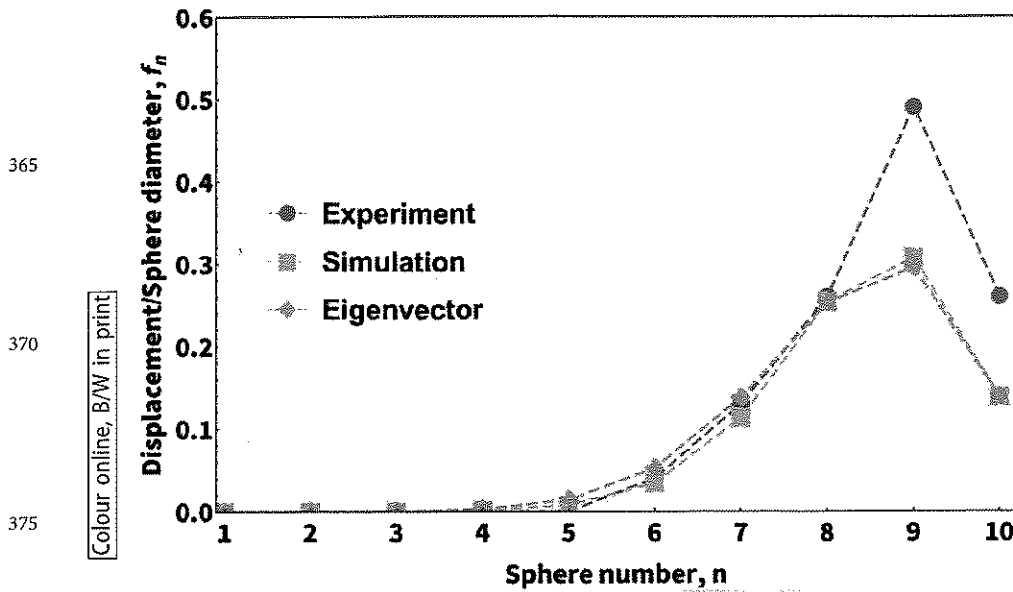

Figure 7. Variation of the three lowest eigenvalues as function of tilt τ, obtained using energy minimisation. The lowest eigenvalue, λ_0, goes to zero linearly at τ_c. The onset of buckling corresponds to the $\lambda_0 = 0$, at τ_c.

Figure 8. The displacement profile of the unstable state at tilt $\tau = 0.031$ as obtained using the iterative method is matched by the Hessian eigenvector of the lowest eigenvalue, λ_0 (normalised, to match the magnitude). Also shown is the experimental data for the friction-arrested state (see discussion in Section 5).

state. The compressive force acting on sphere $N{-}1$ is due to the weight of the linear chain. At the onset of buckling its transverse component, $(\tau(N-2) + \tau(N-1))\sin\theta$ (the sum of the forces due to the contacts with spheres $N{-}2$ and N, respectively), overcomes the restoring force $f = \sin\theta$. It results in the estimate $\tau > (2N-3)^{-1}$ for buckling. It provides a crude, but fairly successful, estimate of τ_c.

A variation of this model allows equal and opposite displacement of the two spheres $N{-}1$ and $N{-}2$ (where sphere N is in contact with the wall). This more accurately describes the effect of localised buckling and captures some of the behaviour of the structure as it approaches the doublet. It leads to an even better estimate for the value of tilt τ_c, at which the unstable solution vanishes,

$$\tau_c = [3(N-2)]^{-1}, \tag{8}$$

see Figure 9.

This trial set of displacements for two spheres involves a single parameter, displacement f, or angle θ, the latter being $\theta = \arcsin f$. The relative energy, Equations (6) and (5), is given by

$$\Delta E(\theta) = \sin^2\theta + \frac{\tau}{3\tau_c}(2\cos\theta + \sqrt{1 - 4\sin^2\theta} - 3). \tag{9}$$
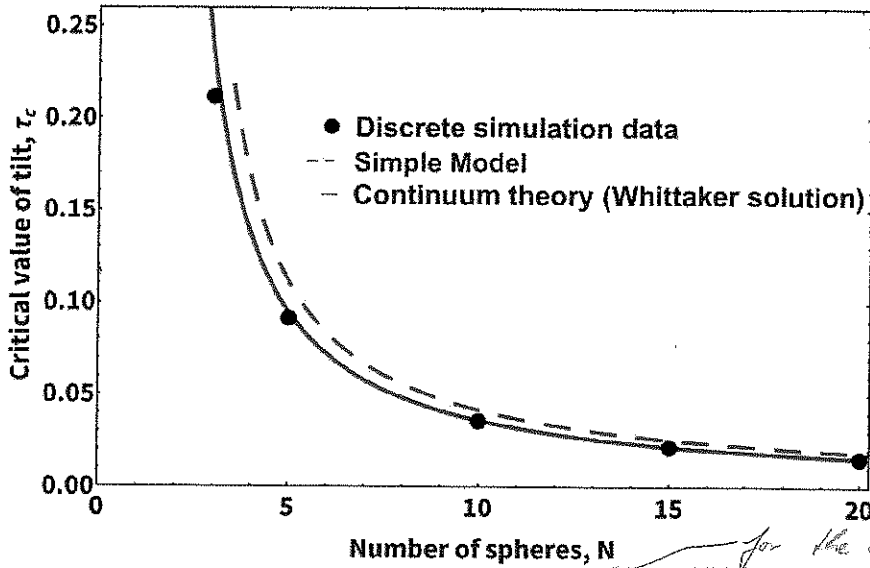
Figure 9. Variation of the critical value of tilt τ_c as a function of the number of spheres, N. The data points are from discrete simulations (iterative method), the solid line is obtained from numerical solutions for the roots of the Whittaker function (a prediction of the continuum model, see Section 4.3), as specified by Equation (12). Also shown is an estimate obtained from a simple ansatz for a displacement profile, Equation (8) (dashed line).

The maximum value of θ is $\pi/6$, which corresponds to the doublet structure. The model is terminated here since it does not have allowance for the additional contacts which arise at that point.

Figure 10 illustrates the form of this function for different values of τ. For $\tau < \tau_c$, the minimum at $\theta = 0$ corresponds to the stable straight chain solution indicated in Figure 4. The maximum corresponds to the unstable solution, discussed in the previous sections, and also represented in Figure 4. For $\tau = \tau_c$ there is only one stationary state, $\theta = 0$ (straight chain), and for $\tau > \tau_c$ it is unstable.

Close to τ_c the amplitude of the unstable solution varies as

$$\theta^2(\Delta\tau) \simeq \frac{2}{3}\left(\frac{\Delta\tau}{\tau_c}\right)\left(1 + \frac{2}{3}\left(\frac{\Delta\tau}{\tau_c}\right)\right), \tag{10}$$

with $\Delta\tau = \tau_c - \tau$. This results in a quadratic variation in energy, for small $\Delta\tau$,

$$\Delta E(\Delta\tau) \simeq \frac{2}{3}\left(\frac{\Delta\tau}{\tau_c}\right)^2\left(1 + \frac{2}{3}\left(\frac{\Delta\tau}{\tau_c}\right)\right). \tag{11}$$

Both scalings are consistent with the results of the discrete simulations, see Figures 5 and 6(b). A deeper analysis of the critical behaviour can be developed using an eigenvalue analysis.
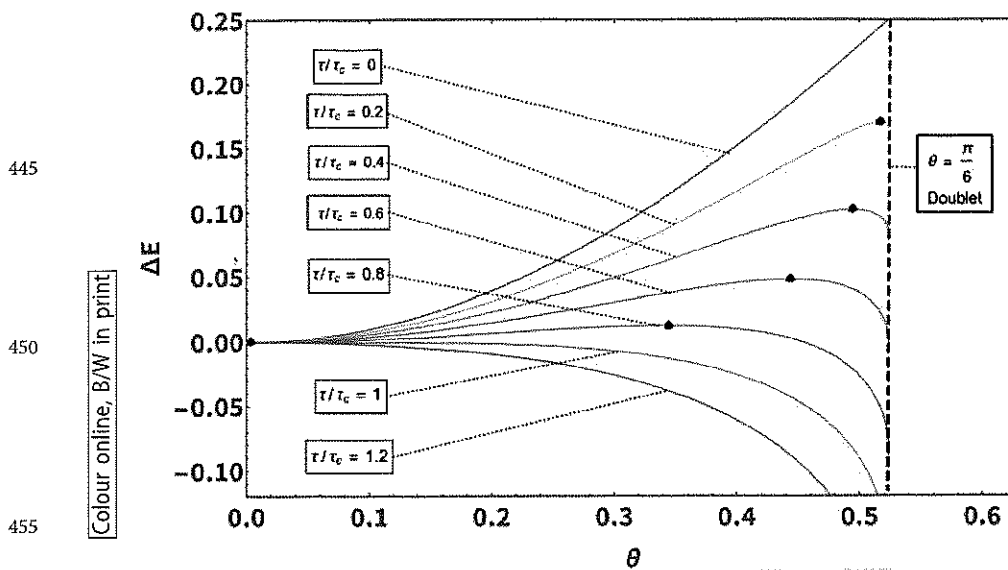
Figure 10. Variation of energy, Equation (9), with angle θ and different ratios τ/τ_c for the simple model, in which only the two penultimate spheres are displaced by $f = \sin\theta$. For values of tilt in the range $0 < \tau/\tau_c < 1$ there are unstable solutions at finite values of θ, marked as black dots. For $\tau/\tau_c \geq 1$ the unstable solution has moved to zero, showing how unstable branch decays as $\tau \to \tau_c$.

We will return to this heuristic model when interpreting our experimental findings in Section 5.

4.3. Continuous formulation

The discrete system may be represented approximately by a continuous formulation, previously used by us to describe buckling under compression [3,5]. This uses the more familiar mathematics of ordinary differential equations. We defer the details of this analysis to a subsequent paper [8], as there is a substantial technical content, but summarise here some of its findings.

In particular, it relates the results at and around the critical point τ_c to Whittaker functions [11] and hence provides a neat analytic formula for τ_c in terms of the properties of this special function. For given N, τ_c is the minimum (positive) value of τ for which

$$M_{\frac{i}{4\tau},\frac{1}{2},4iN} = 0. \tag{12}$$

Here M is the Whittaker function [11] and i is the unit imaginary number. For $N = 10$, this gives $\tau_c = 0.03591\cdots$, as determined numerically using Mathematica. This is remarkably close to the numerical value obtained for the discrete system by simulation: exact agreement is not to be expected. Figure 9 shows close agreement also for other values of N.

Furthermore, the scaling behaviour close to τ_c, as illustrated in Figure 5, is also well described by the continuum theory, the invariant shape of the profile in Figure 6(a) being that of the corresponding Whittaker function with corresponding scaling as in Figure 6(b).

The same Whittaker function can also be used to estimate the critical value of tilt τ_c' for the unstable double-peak solution displayed in Figure 4.

5. Experiments

As we have already indicated, experiments have not yet proved to be fully satisfactory for hard spheres. Nevertheless, such experiments have stimulated much of the analysis presented in this manuscript.

5.1. Experimental set-up and procedure

The experiments were carried out with metal spheres (sets of ball bearings with diameter $D = 9.5$ mm and mass $m = 3.52$ g), confined in a cylindrical perspex tube (diameter $D_T = 34$ mm) which was filled with vegetable oil to reduce friction (see Figure 11). The angle of tilt of the cylinder against the horizontal was determined using a digital spirit level (Neoteck NTK034). The cylinder was sealed with rubber stoppers at both ends; the surface of the stopper in contact with the spheres was covered with a circular plastic sheet to further reduce friction at the contact point.

In these experiments, the restoring transverse force is provided by the curvature of the cylinder. The dimensionless tilt variable τ of Equation (1) is then given by

$$\tau = \frac{1}{2}\left(\frac{D_T}{D} - 1\right)\sin\alpha, \tag{13}$$

as shown in Appendix A.

If one simply tilts such a system, no instability is found until τ is much greater (e.g. by a factor 3 greater) than the τ_c that we have computed for ideal hard spheres. Hence friction is sufficient to hold the system in the unstable straight-chain arrangement of hard spheres, up to a point.

We rule out the use of large perturbations since these tend to force the system into the doublet arrangement over a very wide range of tilts. Instead we have tried to overcome the effects of friction by rolling the tube gently back and forth, thus providing a perturbation of the linear chain.

Our experimental procedure was thus as follows. Starting from an initially linear arrangement of spheres the tube was tilted away from the horizontal by a tilt angle α. This was followed by ten cycles of manually rolling the tube back and forth with a fixed period of 10 seconds and a specified amplitude.

525

530

535

540

545

550
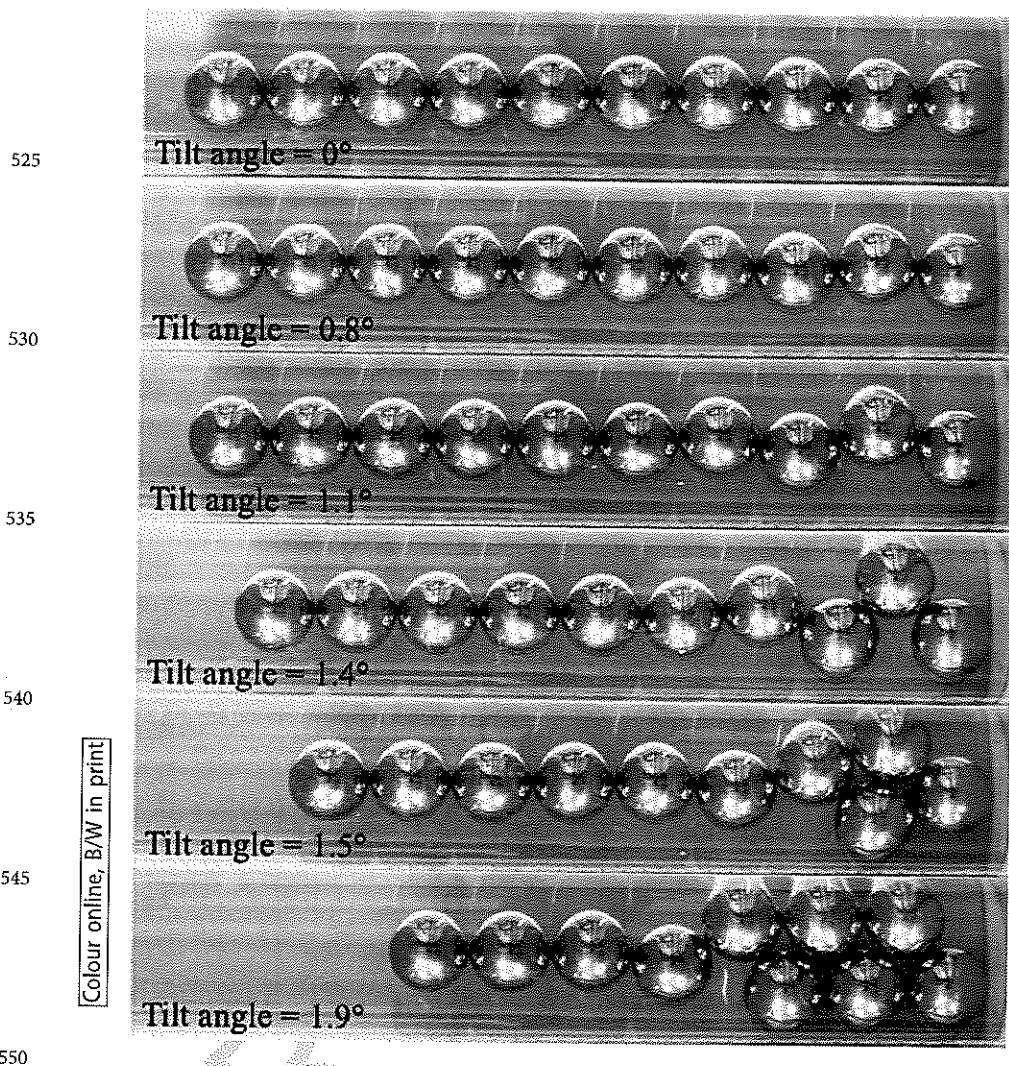
Figure 11. Sphere arrangements obtained using the rolling procedure described in the text. The examples shown are the straight chain (no tilt), buckled single peak structures for tilt angles 0.8, 1.1 and 1.4 degrees, respectively, a 'skewed doublet' structure for 1.5 degrees, and a 'zipper' structure for 1.9 degrees. (The presence of oil in the tubes results in optical distortion. We have corrected for this in these images by re-scaling the photographs by a factor of 2.04 to result in circular shapes for the sphere. Sphere diameter 9.50 mm, inner tube diameter 34 mm, uncertainty in angle measurements, 0.03 degrees. Rolling amplitude, 30 mm.)

555

An image is taken after the rolling is stopped; Figure 11 shows examples of sphere arrangements for six different values of tilt.

560   Image analysis using ImageJ [12] results in profiles of sphere displacement from the tube axis. Experiments were repeated three times for each angle; in each of these runs we started from an initially linear chain.

5.2. Results

We find that once the rolling is stopped, even for values of tilt well below τ_c, the system does *not* return to the linear configuration. The experiments consistently resulted in the formation of a single peak zig-zag configuration, similar in form to the unstable equilibrium state discussed above. An example of the corresponding displacement profiles for the buckled structure is shown in Figure 8. It has all the features of the profiles found in our simulations and is consistent with the profile corresponding to the lowest eigenvalue (see Section 4.1). All profiles are asymmetric, with a maximum displacement at sphere 9, and a substantial displacement also for sphere 10, which is in contact with the flat stopper at the end of the cylinder.

However, while in the frictionless case the displacement amplitude decreases as the critical value of tilt is approached (Figure 6), friction causes the observed displacement to *increase* with tilt, as shown in Figure 12. In Figure 13, we show the maximum displacement (i.e. the displacement of sphere nine) as a function of tilt τ for both our numerical and experimental data. This highlights the different behaviour as the critical point is approached.

The experimental data can be rationalised using the simple model introduced in Section 4.2. A frictional term may be introduced in this model, which arrests its relaxation towards lower energies when $dE/d\theta \leq f$. In the figures which follow, $f = 0.12$. The scenario thus created is shown in Figure 14: note the correspondence of the red curve to that already included in Figure 13.
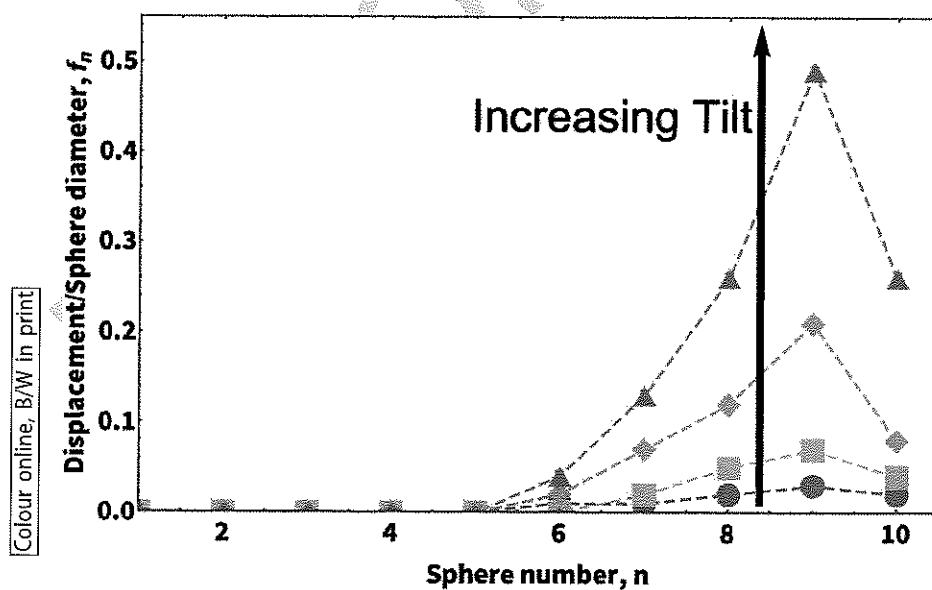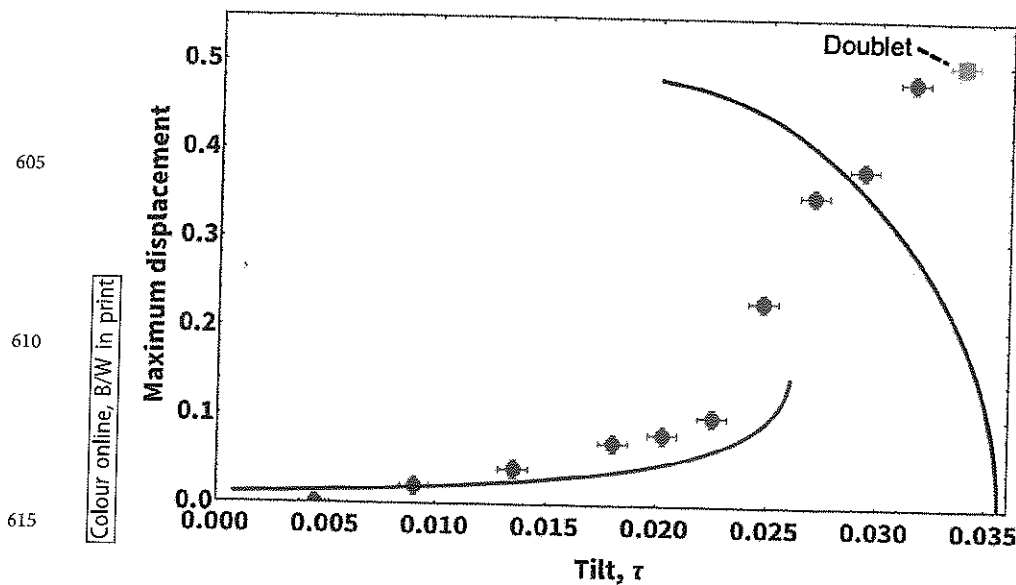

Figure 12. Experimental displacement profiles for (from bottom to top) tilt angles 0.40, 0.80, 1.10 and 1.40 ± 0.03 degrees, corresponding to $\tau = 0.009$, 0.018, 0.024 and 0.0315 (using Equation 13 for conversion).

Figure 13. Contrasting experimental and simulated results for maximum displacement (i.e. corresponding to displacement of sphere 9) as a function of tilt τ. In the simulation (solid blue line) the amplitude of the *unstable* buckled state decreases to zero at the critical value τ_c, where the spheres rearrange to form a doublet structure. In the experiment (data points) the buckled state is friction-arrested, with an increasing amplitude as the doublet is approached. The solid red line is the result of a simple heuristic model, see Figure 14.

In both experiment and this crude theory, upon increase in tilt the single-peak buckled structure eventually becomes unstable and the doublet structure emerges. A further increase in tilt renders also the latter unstable, resulting in what we called the 'zipper structure', see bottom photograph in Figure 11.

6. Conclusion

Simple systems with subtle properties are always interesting. This one proved more so than we expected at the outset. Indeed we identified an unexpected property (the reverse bifurcation), adding to a list of interesting properties previously identified for the buckled linear chain [2,3].

In vague terms, the system presents a type of buckling which, in one form or another, is quite general. Structures that fail under load may do so continuously (although possibly with discontinuous secondary consequences) or *catastrophically*. The latter word has a modern mathematical meaning which may well apply to our case.

In continuing our study we intend to explore the mathematics of the continuum theory mentioned in 4.3, we will include also the case of *combined* tilt and compression [8] in our analysis.

The stability of the linear chain and the presence of the buckled structure in our experimental results serve to highlight the role of friction in arresting

Figure 14. In a simple heuristic model, as described in the text ($f = 0.12$), an initial configuration, displaced from a straight line, is arrested by friction if it lies in the shaded region. In other regions of the diagram, friction is overcome; the system moves as indicated by the arrows, until arrested. This figure shows how the combination of friction and tilt affect a chain with a given initial displacement. The dotted blue line represents the initial maximum displacement of that state, while the dashed blue line shows the observed state. The red line corresponds to that in Figure 13. (The black dashed line is the unstable branch.)

structures that would otherwise be unstable. In this regard, these findings are reminiscent of various columnar structures, composed of tennis balls, that are stable only due to the presence of friction between contacting balls [13].

In conclusion, while our experiments with hard spheres broadly support our numerical and theoretical results, friction makes detailed comparison impossible. We expect that experiments with bubbles [2] will provide a direct experimental counterpart to the theory of this paper, in the foreseeable future.

We will also further explore experiments using of a lathe [1,14]. In that case, the development beyond the zipper (see Figure 11) leads to three dimensional columnar structures [15,16].

Disclosure statement

No potential conflict of interest was reported by the author(s).

Funding

ORCID

A. Irannezhad http://orcid.org/0000-0002-7297-2023

References

[1] J. Winkelmann, A. Mughal, D. Weaire, and S. Hutzler, *Equilibrium configurations of hard spheres in a cylindrical harmonic potential*, EPL (Europhys. Lett.) 127(4) (2019), pp. 44002.

[2] D. Weaire, A. Irannezhad, A. Mughal, and S. Hutzler, *A simple experimental system to illustrate the nonlinear properties of a linear chain under compression*, Am. J. Phys. 88 (5) (2020), pp. 347–352.

[3] S. Hutzler, A. Mughal, J. Ryan-Purcell, A. Irannezhad, and D. Weaire, *Buckling of a linear chain of hard spheres in a harmonic confining potential: Numerical and analytical results for low and high compression*, Phys. Rev. E. 102(2) (2020), pp. 022905.

[4] A. Mughal, D. Weaire, and S. Hutzler, *Peierls–Nabarro potential for a confined chain of hard spheres under compression*, EPL (Europhys. Lett.) 135 (2021), pp. 26002.

[5] D. Weaire, A. Mughal, J. Ryan-Purcell, and S. Hutzler, *Description of the buckling of a chain of hard spheres in terms of Jacobi functions*, Physica. D. 433 (2022), pp. 133177.

[6] H. Landa, B. Reznik, J. Brox, M. Mielenz, and T. Schätz, *Structure, dynamics and bifurcations of discrete solitons in trapped ion crystals*, New. J. Phys. 15(9) (2013), pp. 093003.

[7] I. Georgescu, *Trapped ion quantum computing turns 25*, Nat. Rev. Phys. 2(6) (2020), pp. 278–278.

[8] S. Hutzler, D. Weaire, A. Mughal, and J. Ryan-Purcell, Continuum description of the buckling of a chain of hard spheres under tilt, (in preparation), (2022).

[9] M. van Hecke, *Jamming of soft particles: Geometry, mechanics, scaling and isostaticity*, J. Phys. Condens. Matter. 22(3) (2009), pp. 033101.

[10] G.T. Pickett, M. Gross, and H. Okuyama, *Spontaneous chirality in simple systems*, Phys. Rev. Lett.85 (17) (2000), pp. 3652–3655.

[11] M. Abramowitz and I.A. Stegun, Handbook of Mathematical Functions, Dover Publications, New York, 1965. Section 13.1.32.

[12] C.A. Schneider, W.S. Rasband, and K.W. Eliceiri, *NIH image to ImageJ: 25 years of image analysis*, Nat. Methods. 9 (7) (2012), pp. 671–675.

[13] A. Rogava, *Tennis-ball towers*, Physics. World. 32(5) (2019), pp. 25.

[14] T. Lee, K. Gizynski, and B.A. Grzybowski, *Non-Equilibrium Self-Assembly of monocomponent and multicomponent tubular structures in rotating fluids*, Adv. Mater. 29 (47) (2017), pp. 1704274.

[15] L. Fu, W. Steinhardt, H. Zhao, J.E. Socolar, and P. Charbonneau, *Hard sphere packings within cylinders*, Soft. Matter. 12(9) (2016), pp. 2505–2514.

[16] H.K. Chan, Y. Wang, and H. Han, *Densest helical structures of hard spheres in narrow confinement: an analytic derivation*, AIP. Adv. 9(12) (2019), pp. 125118.

Appendix A. The non-dimensional tilt variable τ for hard sphere experiments

In our experiments with hard spheres the restoring transverse force is provided by the curvature of the cylinder, see Figure A1. Transverse displacement Y of a sphere of mass m is opposed by a gravitational force $(2Ymg/(D_T - T))[1 - 4(Y/(D_T - D))^2]^{-1/2} \simeq (2Ymg/(D_T - T))(1 + 2(Y/(D_T - D))^2)$, where D_T and D are cylinder and sphere diameter, respectively. The maximum displacement is about $D/2$ (doublet structure) and we thus obtain $2(Y/(D_T - D))^2 \simeq 0.08 \ll 1$. The restoring force is thus approximated linear in displacement Y with a force constant k_p of

$$k_p = 2\,mg/(D_T - D).\qquad(A1)$$

In a cylinder tilted by an angle α against the horizontal, a sphere exerts a longitudinal force $mg\sin\alpha$ on its contacting neighbouring (in the direction of tilt) sphere. As in our modelling of the discrete system, we introduce τ as a non-dimensional tilt variable via
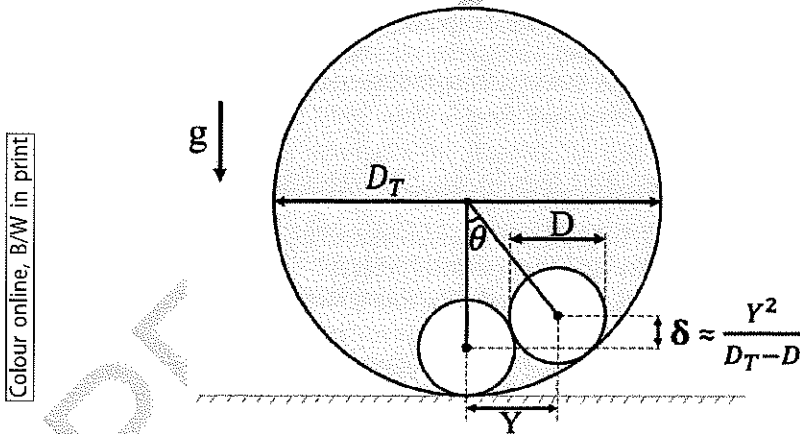
$$\tau = mg\sin\alpha/(k_p D).\qquad(A2)$$

Inserting for k_p (Equation A1), we obtain

$$\tau = \frac{1}{2}\left(\frac{D_T}{D} - 1\right)\sin\alpha.\qquad(A3)$$

Figure A1. Diagram showing the geometry of the hard spheres held against the curved surface of the tube, which can be used to relate the physical dimensions of the system to k_p, the (approximate) spring constant of the confining potential (see also [2]).